NJC

PAPER

View Article Online
View Journal

Cite this: DOI: 10.1039/c5nj01103e

Binding of a potential anti-hepatoma drug *cis,cis,trans*-[Pt(NH$_3$)$_2$Cl$_2$(O$_2$CCH$_2$CH$_2$COOH)-(OCONHC$_{16}$H$_{33}$)] with serum albumin – thermodynamic and conformational investigations†

Li Qi, Zhong Lu,* Wen-hua Lang, Lu Guo, Chang-geng Ma and Guang-hong Sun

Received (in Montpellier, France)
24th July 2015,
Accepted 14th September 2015

DOI: 10.1039/c5nj01103e

www.rsc.org/njc

In this paper, a potential anti-hepatoma Pt^{4+} drug *cis,cis,trans*-[Pt(NH$_3$)$_2$Cl$_2$(O$_2$CCH$_2$CH$_2$COOH)-(OCONHC$_{16}$H$_{33}$)] was synthesized and selected to investigate its binding to human serum albumin (HSA) by spectroscopy and molecular docking methods. Fluorescence spectra show that the Trp residue, the intrinsic fluorophore in HSA, was induced to a less hydrophobic microenvironment with the addition of the Pt^{4+} compound, which induces the denaturation of HSA. Moreover, the fluorescence quenching mechanism was determined to be static quenching. The binding constant (K_A) and the number of binding sites (n) were calculated based on the results of fluorescence measurements. Circular dichroism (CD), Fourier transform infrared spectroscopy (FTIR) and three dimensional fluorescence spectroscopy proved that the Pt^{4+} compound could slightly change the secondary structure and induce unfolding of the polypeptides of protein. Thermodynamic parameters indicate that the Pt^{4+} compound binds to HSA through electrostatic attraction with one binding site. The molecular docking study indicated that parecoxib is embedded into site I (subdomain IIA) of HSA.

1. Introduction

Platinum-based compounds are among the most active chemotherapeutic agents available. They are effective against a multitude of cancers. Cisplatin is one of the most effective drugs in the treatment of solid tumors including epithelial ovarian carcinoma, head and neck squamous carcinoma.[1–3] It exerts its cytotoxic action by forming intra- and interstrand adducts with DNA, which induce apoptosis thereafter. However, dose-limited side effects of cisplatin narrow its clinical use. Therefore, it would be advantageous to increase the therapeutic index of cisplatin by increasing its efficacy or decreasing the toxic side effects. In order to do this, nowadays, much attention regarding platinum anti-cancer drugs has been paid to Pt^{4+}-based compounds.[4–8] There are many Pt^{4+} compounds that have been synthesized and their anti-cancer activities have been evaluated.[5,7,9,10] As a result, the Pt^{4+} compounds have been proven to have advantages over the Pt^{2+} compounds because of their kinetic inertness and thus toxicity is less compared to their Pt^{2+} counterparts. Because Pt^{4+} is the most potent member of the Pt anticancer drug family, its potential use in liver cancer is attractive.

As the most abundant protein in the circulatory system, human serum albumin (HSA) possesses many unique physiological and pharmacological functions in human body.[11–13] The protein was reported to serve as a transporter for a variety of endogenous and exogenous compounds such as drugs, fatty acids and dyes in the bloodstream. The binding between anti-cancer drugs and HSA can significantly affect the absorption, distribution, metabolism and toxicity of the drugs, and may change the functions and structures of the protein. Thus, the investigations on the interaction of HSA with anti-cancer drugs are not only important to comprehend their transport and metabolism processes in the body, but also can provide insight into the understanding of the toxicity of the drugs at the molecular level.

In the present work, we synthesized a potential Pt^{4+} anti-hepatoma drug *cis,cis,trans*-[Pt(NH$_3$)$_2$Cl$_2$(O$_2$CCH$_2$CH$_2$COOH)-(OCONHC$_{16}$H$_{33}$)]. Multispectroscopic methods including fluorescence, UV-vis absorption and circular dichroism (CD) spectroscopy, coupled with a molecular docking technique were employed to characterize the binding of the Pt^{4+} compound with HSA and the effect of the Pt^{4+} compound on the molecular

Clinical College of Weifang Medical University, Weifang 261031, China.
E-mail: luzhongdoc1103@hotmail.com; Fax: +86-05368068895;
Tel: +86-05368068895

† Electronic supplementary information (ESI) available. See DOI: 10.1039/c5nj01103e

conformation of HSA at physiological pH (pH 7.4). The study provides a quantitative understanding of the effect of the Pt^{4+} compound on the structure of HSA, which could be useful supports for the further design of a much more suitable Pt^{4+} compound with structural variants.

2. Materials and methods

2.1. Materials

HSA with a sharp molecular weight distribution at 66 400 g mol^{-1} was purchased from Amresco. Cisplatin was obtained from Hubei Biocause Pharmaceutical Co., Ltd (Hubei, China; purity no less than 99.7%). Phenylbutazone (99% purity) was purchased from ACROS ORGANICS (New Jersey, USA); ibuprofen (99% purity) was purchased from Shanghai Civi Chemical Technology Co., Ltd (Shanghai, China); and digitoxin (99% purity) was purchased from Hubei Huabei Biomedicine Co., Ltd (Wuhan, China). All other chemicals were bought from Sinopharm Co., Ltd (Beijing, China).The pH value of the mixture solutions for the tests was 7.4. It should be noted that, since the isoelectric point of HSA occurs at 4.9, under this condition it is in a negative form.

2.2. Methods

The asymmetrically functionalized Pt^{4+} compound 3 can be obtained by the reaction of 2 with succinic anhydride using the method from Dhar[14] as described in Fig. 1. Compound 3 was placed into a 5 mL glass vial and the isocyanate $C_{17}H_{35}NO_2$ (anhydrous DMF) solution (2 mL) was added. The suspension was stirred overnight. The next day, the suspension had become a clear green solution. The solution was then filtered and the solvent was removed under reduced pressure at 65 °C. Ethyl ether (2 mL) was added to the oily residue, and the mixture was ultrasonicated for 1 min and centrifuged. The solid was further washed with DCM (4 mL) and diethyl ether (2 mL). The washed solid was then left under vacuum overnight.

The human ovarian carcinoma A2780, cisplatin resistant A2780/CP70 cell lines and the human lung carcinoma cell line A549 were kindly provided by Dr Sufang Zhang. Cytotoxicity against different cell lines (A549, A2780, and A2780/CP70) was evaluated by the MTT assay. Cells were seeded on a 96 well plate (2000 cells per well) in 200 μL RPMI or DMEM and incubated for 24 h at 37 °C. The following day, solutions of the platinum compounds were freshly prepared in RPMI or DMEM media (Pt^{4+} compound), PBS (cisplatin), or obtained by FPLC isolation and quantitated by GFAAS. Preparation of the samples for the Pt^{4+} compound was achieved by ultrasonication of a suspension of the solid platinum complex in cell culture medium for 30 min followed by filtration through a 0.2 μM syringe filter. The cells were then treated with the platinum compounds, separately at varying concentrations, and incubated for 72 h at 37 °C. The cells were then treated with 200 μL fresh medium containing 3-(4,5-dimethylthiazol-2-yl)-2,5-diphenyltetrazolium bromide (MTT) (0.8 mg mL^{-1}) and incubated for 3 h at 37 °C. The medium was removed, 200 μL of DMSO was added to the cells, and the absorbance of the purple formazan was recorded at 570 nm using a BioTek Synergy HT multi-detection microplate plate reader. Each experiment was performed in triplicate for each cell line.

Fluorescence spectral analysis was carried out on a Hitachi F-4500 fluorescence spectrophotometer using 1.0 cm quartz cells. The excitation wavelength of HSA studied in this work was 280 nm. Synchronous fluorescence spectra were acquired by the same spectrofluorometer. They were recorded and the difference between excitation wavelength and emission wavelength was kept constant ($\Delta\lambda = \lambda_{em} - \lambda_{ex}$). When the $\Delta\lambda$ was at 15 or 60 nm, the synchronous fluorescence spectrum gave the characteristic information about Tyr residues or Trp residues. All the excitation and emission slits were set at 5/5 nm. The experiments were carried out at 298 K.

CD spectra were recorded over a wavelength range of 190–250 nm at 0.2 nm intervals at 298 K in a thermostated cell holder on a MOS-450 CD spectrometer. The scanning speed was set at 200 nm min^{-1} and the cell length was 1 cm. Results are expressed as ellipticity (mdeg), which was obtained in mdeg directly from the instrument. Three scans were made and averaged for each CD spectrum.

Fluorescence lifetimes have been measured using a time-correlated-single-photon counting (TCSPC) spectrophotometer (Horiba Jobin Yovin) with full width at half maximum (FWHM)

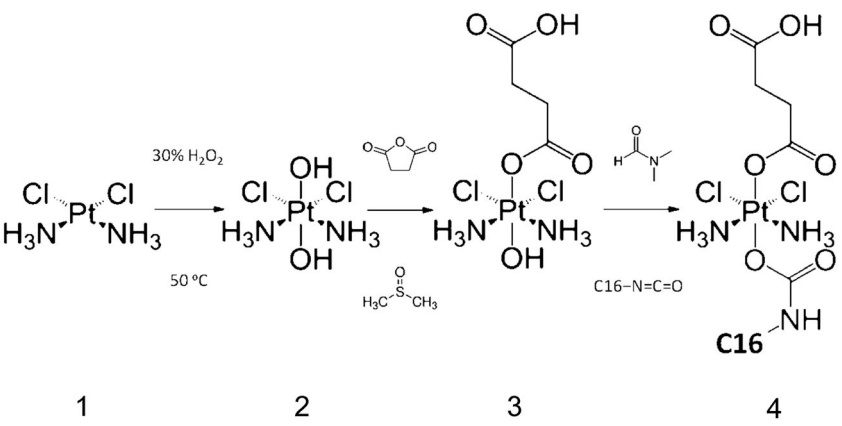

Fig. 1 Route of Pt^{4+} compound synthesis.

ca. 300 ps, repetition rate 1 MHz and the resolution was 28 ps per channel. The excitation and emission wavelengths have been chosen to be 280 and 340 nm, respectively and MCP-PMT as a detector. The emission from the samples was collected at a right angle to the direction of the excitation beam maintaining magic-angle polarization (54.7°). The data have been fitted to multiexponential functions after deconvolution of the instrument response function by an iterative reconvolution technique using IBH DAS 6.2 data analysis software in which reduced χ^2 serves as a parameter for goodness of fit.

Measurements of FT-IR were carried out on a Nicolet Avatar 330 FT-IR spectrometer equipped with a germanium attenuated total reflection (ATR) accessory, adeuterated triglycine sulfate (DTGS) detector, and a KBr beam splitter. All the FT-IR spectra were taken *via* the ATR method with a resolution of 4 cm^{-1} and 128 scans at room temperature. The background (containing all system components except protein) was collected under the same conditions and subtracted from the spectra of sample solution to obtain the FT-IR spectra of protein.

The PDB entry of the HSA crystal structure employed in the docking study was 1H9Z. The docking study was conducted by a Surflex Dock program in Sybyl 8.1 package. The protocol was generated by residues and ligand mode. The threshold was set at 0.50, while the bloat was 0. The parameters in the docking work were set as follows: additional starting conformation per molecule: 20; angstroms to expand search grid: 6; max conformation per fragment: 20; max number of rotatable bonds per molecule: 100. The structure of the Pt^{4+} compound was drawn by Sybyl 8.1 package. After being charged using the Gasteiger and Marsili method, the molecule was optimized in energy and geometry using Tripos Force Field.

3. Results and discussion

3.1. Synthesis of the Pt^{4+} compound

The amphiphilic Pt^{4+} compound construct was prepared using the synthetic approach shown in Fig. 1. Hydrogen peroxide oxidation of cisplatin (1) in water affords 2. The asymmetrically functionalized Pt^{4+} compound 3 can be obtained by the reaction of 2 with succinic anhydride. The fortuitous acetone solubility of the disuccinate compound and the insolubility of 3 provide an effective means of removing the undesired side product.[14] The ability of isocyanate reagents to undergo nucleophilic attack by the platinum-bound hydroxide ligand of 3 was exploited to form a Pt^{4+} carbamate species. Compound Pt^{4+} bear a hydrophobic unbranched aliphatic chain with a length of C16.

The Pt^{4+} compound was fully characterized by multinuclear (1H, 13C, and 195Pt) NMR spectroscopy and electrospray ionization mass spectrometry (ESI-MS) (Fig. S1, ESI†). The Pt^{4+} compound displays a 195Pt NMR signal around δ = 1240 ppm, confirming the 4+ oxidation state of the platinum. In the ESI mass spectra, well defined isotopic distribution patterns provided further confirmation of chemical composition. Chemical purity was established with combustion analysis and analytical HPLC (Fig. S2, ESI†), which shows that the Pt^{4+} compound takes more than 95% in the final product.

3.2. Cytotoxicity and uptake of the Pt^{4+} compound

The cytotoxicity of the Pt^{4+} compound and cisplatin was examined using the on-target CCRF-CEM leukaemia cell line and the off-target ovarian carcinoma cell line A2780 and its cisplatin-resistant derivative A2780/cp70. Cancer cells were treated with cisplatin or Pt^{4+} compound for 48 h and cell viability was evaluated. IC_{50} values, which represent the concentration required to inhibit growth by 50%, are given in Fig. 2A. The IC_{50} for cisplatin at 48 h is 0.92 ± 0.04 μM, and that for the Pt^{4+} compound is 0.33 ± 0.03 μM. In addition, we further evaluated the cytoxicity of the Pt^{4+} compound in normal human cells. The IC50 value of the Pt^{4+} compound in the MRC-5 (normal lung tissue) cell line is 0.74 ± 0.05 μM, which is two times that in the A2780 ovarian cancer cell lines (IC_{50} = 0.33 ± 0.03 μM).

The extent of cellular uptake was investigated by treating A2780 ovarian cancer cells with 5 μM of cisplatin or Pt^{4+} compound for 5 h. The whole cell concentration of platinum was then evaluated by inductively coupled plasma mass spectrometry. Notably, from cisplatin to Pt^{4+} compound, the 34.57-fold increase in cellular uptake is mirrored by increase in cytotoxicity, suggesting that the increase in cytotoxicity can be attributed in large part to the increase in uptake. As shown in Fig. 2A, the Pt^{4+} compound also displays a lower resistance factor in ovarian cancer cell lines than cisplatin, and the treatment with cisplatin or Pt^{4+} compound at equimolar concentrations led to drastically different degrees of cell survival.

3.3. Quenching mechanism, binding number and affinity determination of the protein-compound system

Analysis of Trp fluorescence quenching for the determination of interactions between the Pt^{4+} compound with HSA were performed through titration of the Pt^{4+} compound against protein. Fig. 3A shows that HSA has a strong fluorescence emission peak at ~340 nm. Thus, following quenching of the HSA fluorescence on addition of the compound can conclude

(A)

	IC_{50} (μM)			
Compound	Cell line			
	CCRF-CEM	A2780	A2780/cp70	Resistance
Cisplatin	0.62±0.04	0.92±0.04	5.15±0.05	5.59
Pt (IV) drug	0.14±0.05	0.33±0.03	0.22±0.02	0.67

(B)

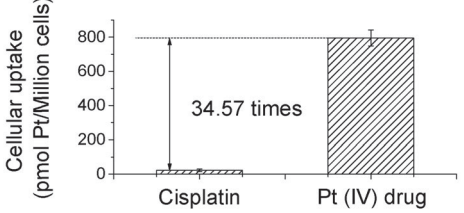

Fig. 2 (A) The *in vitro* cytotoxicity using growth inhibition assays of the compounds after 48 h of exposure. (B) Whole cell uptake of the compounds. Error bars are the standard deviations of three runs.

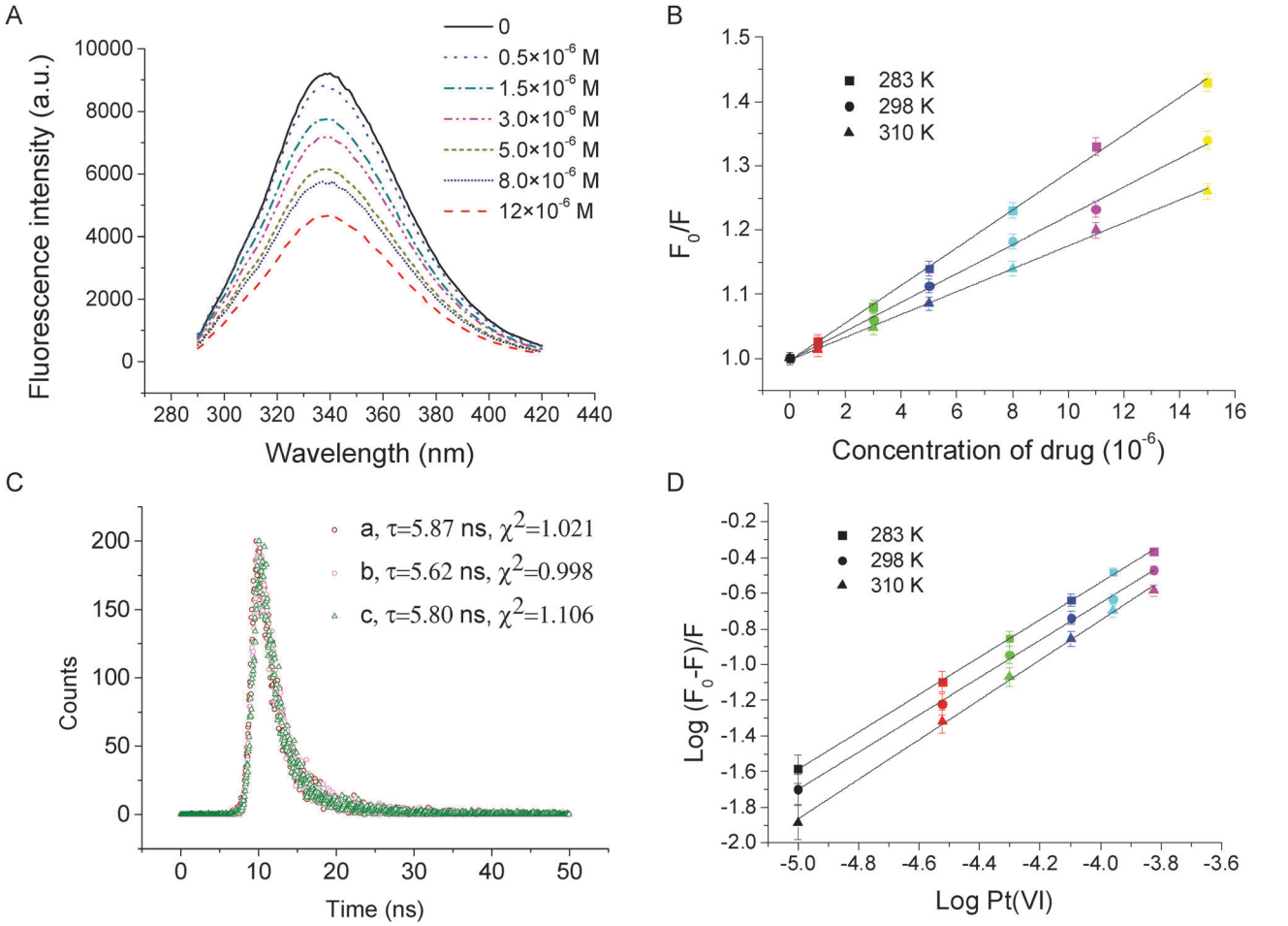

Fig. 3 (A) Effect of the Pt^{4+} compound on the fluorescence intensity of HSA. (B) Stern–Volmer and (D) Hill plots for HSA interacting with the Pt^{4+} compound at 283 K, 298 K, and 310 K. Conditions: T = 298 K, pH 7.4, salt concentration 0.9%; c(HSA) = 1.0 × 10^{-6} M; $c(Pt^{4+})$: 0, 1.0, 3.0, 5.0, 8.0, 11.0, and 15.0 × 10^{-5} M. (C) The time-resolved fluorescence decay for HSA interacting with the Pt^{4+} compound at 298 K, pH = 7.4, salt concentration 0.9%. c(HSA) = 1.0 × 10^{-6} M; $c(Pt^{4+})$ 1–3: 0, 5.0 and 15.0 × 10^{-5} M. Error bars are the standard deviations of three runs.

whether the Pt^{4+} compound interacts with the protein at the site close to Trp-214. There is a continuous decrease in the emission spectral intensity of HSA without significant change in the wavelength of maximal fluorescence emission (λ_{max}). The decrease in fluorescence intensity upon addition of the compound was analyzed according to the Stern–Volmer equation:[12] $F_0/F = 1 + K_q\tau_0[Q] = 1 + K_{SV}[Q]$, where F_0 and F are the fluorescence intensities in the absence and presence of the quencher, respectively. K_q and K_{SV} are the quenching rate constants of the bimolecular and the Stern–Volmer dynamic quenching constant, respectively. [Q] is the concentration of the quencher and τ_0 is the average lifetime of HSA without a quencher.

Fluorescence quenching can be either dynamic or static in nature. To know about the quenching mechanism of HSA by the Pt^{4+} compound, we analyzed the data by the Stern–Volmer plots (Fig. 3B). K_q is 2.24 × 10^{12} M^{-1} s^{-1}, which lies in the order of 10^{12}, as shown in Table 1. However, the K_q for the HSA–Pt^{4+} compound system is 100 times higher than the maximum scatter collision quenching constant of various quenchers with polymers (2 × 10^{10} M^{-1} s^{-1}). This shows that quenching is not initiated by dynamic diffusion but occurs by the formation of a strong complex between HSA and the Pt^{4+} compound. Furthermore, the temperature dependence of K_{SV} is studied to distinguish the type of quenching by the differential response toward

Table 1 Stern–Volmer quenching constants, binding parameters, and thermodynamic parameters of the HSA–Pt^{4+} drug system at different temperatures

	Stern–Volmer quenching constants			Binding parameters			Thermodynamic parameters		
T (K)	K_q (M^{-1} s^{-1})	K_{SV} (M^{-1})	R	K_A (M^{-1})	n	R	ΔG° (J mol^{-1})	ΔS° (J mol^{-1} K^{-1})	ΔH° (J mol^{-1})
283	2.93 × 10^{12}	2.93 × 10^4	0.9968	5.07 × 10^3	1.11	0.9998	−2.01 × 10^4		
298	2.24 × 10^{12}	2.24 × 10^4	0.9976	4.51 × 10^3	1.05	0.9991	−2.08 × 10^4	33.5	−1.07 × 10^4
310	1.78 × 10^{12}	1.78 × 10^4	0.9973	3.37 × 10^3	1.05	0.9992	−2.09 × 10^4		

temperature and viscosity. In static quenching, K_{SV} decreases with an increase in temperature due to the formation of complex with protein, which undergoes dissociation on increasing temperature. However, for dynamic quenching, K_{SV} increases with temperature as in this case higher temperature results in faster diffusion of the quencher and hence larger extent of collisional quenching.[15] We found that upon increasing temperature, the K_{SV} value decreases, which is good indication of static quenching.

Time-resolved fluorescence spectroscopy is a tool that can probe the interaction between ligands and proteins. The fluorescence lifetime can be used to directly distinguish between dynamic and static quenching. For static quenching, the lifetime does not depend on the quencher concentration (*i.e.*, $\tau_0 = \tau$). Time resolved fluorescence spectra of the free HSA and HSA–Pt^{4+} complexes are shown in Fig. 3C using the fluorescence decay parameters. The fluorescence decay of the unquenched protein is almost the same with the quenched protein. The average fluorescence lifetime of Trp-214 stayed still with increasing Pt^{4+} compound. These results suggested that the HSA–Pt^{4+} compound quenching mechanism was static.

When small molecules bind independently to a set of equivalent sites on a macromolecule, the binding number between them has also been studied through the following double-logarithmic equation:[16,17]

$$\lg\frac{F_0 - F}{F} = \lg K_A + n\lg[Q]$$

where F_0 and F stands for the fluorescence intensity in the absence and the presence of the quencher at various concentrations of $[Q]$ respectively, K_A refers to the binding constant, and n is the binding number. According to the equation, the binding number can be obtained from the slope of the plot of lg $(F_0/F - 1)$ *vs.* lg$[Q]$ (Fig. 3D). Table 1 demonstrates that the value of n is close to 1 and K_A is in the order of 10^3, which suggests that the Pt^{4+} and HSA have one binding site and exhibits a weak binding force during their interaction process. In general, the interaction forces between ligands and proteins may include electrostatic interactions, multiple hydrogen bonds, van der Waals interactions, hydrophobic and steric contacts within the antibody-binding site, *etc.* To elucidate the interaction between the Pt^{4+} compound and HSA, the temperature-dependent thermodynamic parameters were calculated from the van't Hoff plots. It is supposed that the enthalpy change (ΔH) does not vary significantly in the temperature range studied and can be considered as a constant, then both the enthalpy change (ΔH) and entropy change (ΔS) can be evaluated from the van't Hoff equation:[18]

$$\ln K = -\frac{\Delta H}{RT} + \frac{\Delta S}{R}$$

where K is analogous to the effective quenching constants at the corresponding temperatures and R is the gas constant (8.314 J mol^{-1} K^{-1}). The temperatures used in our experiment were 283, 298 and 310 K. From Fig. 4 we can see that the linear relationship between ln K and $1/T$ is good. The enthalpy change (ΔH) is obtained from the slope of the van't Hoff relationship,

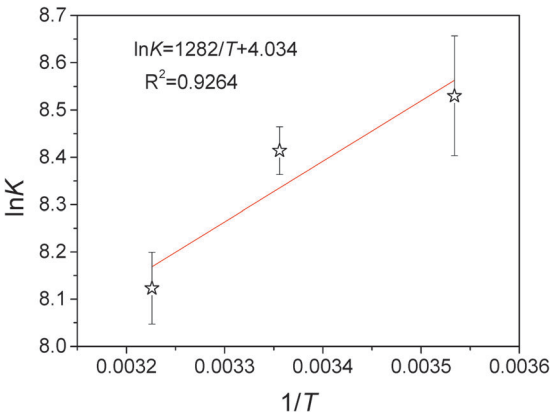

Fig. 4 van't Hoff plot for the HSA–Pt^{4+} compound system. Error bars are the standard deviations of three runs.

while the free energy change (ΔG) is then calculated from the following relationship: $\Delta G = \Delta H - T\Delta S = -RT\ln K$. The corresponding results were presented in Table 1, while the values of ΔH and ΔS of the binding site were obtained from the slopes and ordinates at the origin of fitted lines. The values of ΔH and ΔS are found to be -1.07×10^4 J mol^{-1} and 33.5 J mol^{-1} K^{-1}, which indicated that the electrostatic force played the major role in the process of forming the Pt(IV) complex.[19,20] This was also confirmed by the salt effect experiments (Fig. S3, ESI†). The negative sign for ΔG means that the binding process is spontaneously driven by enthalpy and entropy together.

3.4. Conformational changes of HSA induced by the Pt^{4+} compound

Synchronous fluorescence spectra can give information about the molecular environment in the vicinity of chromosphere molecules in low concentrations under physiological conditions. It is a sensitive technique for detecting microenvironmental changes in these chromophores, with several advantages, such as spectral simplification, spectral bandwidth reduction and avoiding different perturbing effects. When the D values ($\Delta\lambda$) between excitation and emission wavelengths are stabilized at 15 or 60 nm, synchronous fluorescence gives the characteristic information about Tyr or Trp residues.[21] The effect of the Pt^{4+} compound on HSA synchronous fluorescence spectra is shown in Fig. 5, from which it is apparent that the maximum emission wavelength had a slight red shift of 5 nm in the investigated concentration range when $\Delta\lambda$ = 60 nm, which suggested a more polar (or less hydrophobic) environment of Trp residues; while when $\Delta\lambda$ = 15 nm the maximum emission wavelength moved only 2 nm at the investigated concentration range, which indicated that there was less change in the microenvironment of Tyr residues. FT-IR spectroscopy has emerged as an established technique to investigate the structural characteristics of proteins. Among the amide bands of the protein, the amide I band (1700–1600 cm^{-1}, mainly C═O stretch) and amide II band (1600–1500 cm^{-1}, C–N stretch coupled with N–H bending mode) both have a relationship with the secondary structure of protein, which range from gross aspects to subtle rearrangements

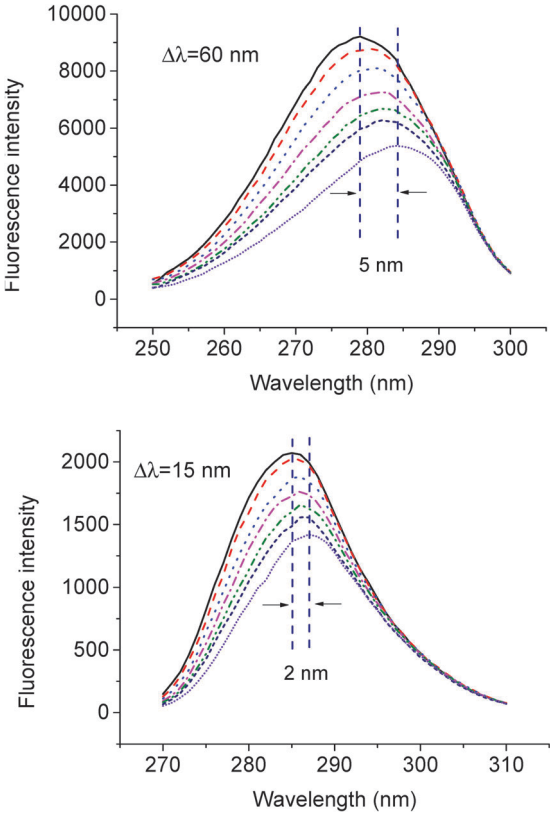

Fig. 5 Synchronous fluorescence spectra of the Pt^{4+} compound with HSA with $\Delta\lambda$ = 15 nm or $\Delta\lambda$ = 60 nm at 298 K. Concentrations are consistent with the steady-state fluorescence study.

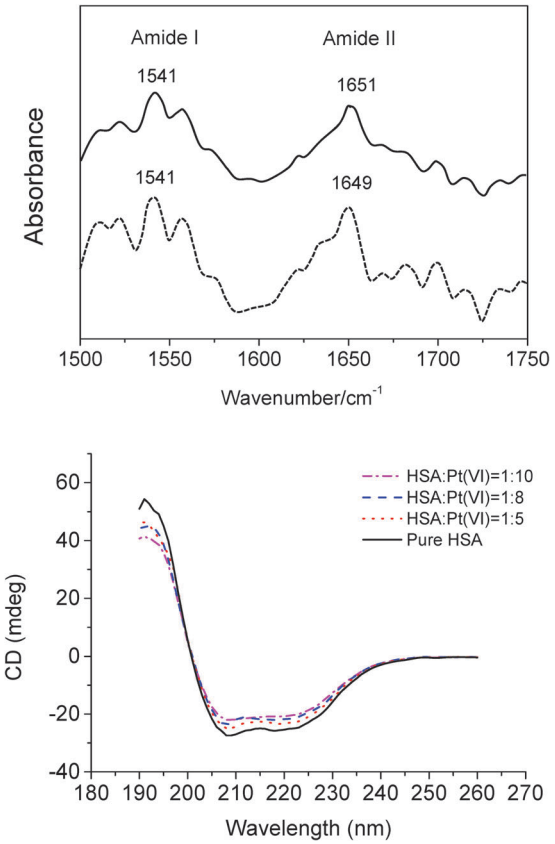

Fig. 6 Upper: FT-IR spectra of free HSA (solid curve, 1.0×10^{-4} M), the HSA–Pt^{4+} compound complex (the molar ratio of HSA/Pt^{4+} compound was maintained at 1 : 3 for the dashed curve). Lower: CD spectra of HSA in the absence and presence of Pt^{4+} compound. The concentration of HSA was 2.0×10^{-7} M, and the concentrations of the Pt^{4+} compound were 0 (a), 2.0 (b) and 5.0 (c) $\times 10^{-7}$ M. T = 298 K, pH = 7.4, salt concentration 0.9%.

associated with ligand binding. In the infrared spectra, the amide I region occur approximately at 1600–1700 cm^{-1}, while the amide II region occurs nearly at 1548 cm^{-1}. The former region appears due to the C═O stretching vibration, which has significantly higher signal intensity; the later one occurs due to C–N stretch coupled with N–H bending. The conformational sensitivity of amide bands is primarily due to the hydrogen bonding and the coupling between transition dipoles. Fig. 6(upper) compares the FT-IR spectra of HSA and the difference spectra of HSA–Pt^{4+} complex in phosphate buffer solution at 298 K. The difference spectra of the HSA–Pt^{4+} complex were obtained by subtracting the spectra of the Pt^{4+} compound from the spectra of the HSA–Pt^{4+} complex. The shift in the peak position of the amide I band of HSA from 1651 to 1649 cm^{-1} after addition of the Pt^{4+} compound indicates the change around the amido bond (C═O) of HSA upon interaction with the Pt^{4+} compound. Analysis of the secondary structure of HSA and Pt^{4+} complex was carried out on the basis of the CD technique. The CD spectra of HSA in the absence and presence of the Pt^{4+} compound were shown in Fig. 6. As Fig. 6(lower) showed, HSA exhibited two negative ellipticities at 208 and 220 nm in the UV region, which were characteristic of the typical α-helix structure of protein.[22] The binding of the Pt^{4+} compound to HSA caused a decrease in band intensity at all wavelengths of the far-UV CD without any significant shift of the peaks, indicating the decrease of the α-helical content in protein, which means the peptide strand unfolding even more. However, the CD spectra of HSA in the presence and absence of the Pt^{4+} compound are similar in shape, indicating that the structure of HSA is also predominantly α-helical. From the above results, it is apparent that the effect of the Pt^{4+} compound on HSA causes a conformational change of the protein, with the loss of α-helical stability.[23,24] The calculating results exhibited a reduction of α-helix structures from 58.4% of native protein to 52.6% at molar ratio Pt^{4+} compound/HSA = 10 : 1, while the fractions of random coil increased from 20.6% to 25.3%, indicating the adaptive structural alterations (Table 2).[25]

The three-dimensional fluorescence spectra are used to further study the change in the configuration of proteins induced by small molecules. The three-dimensional fluorescence

Table 2 Secondary structural content of HSA in the absence and presence of the Pt^{4+} drug

	Content (%)			
Sample	α-Helix	β-Sheet	β-Turn	Random coil
Pure HSA	58.4	10.3	10.7	20.6
HSA : Pt^{4+} = 1 : 5	55.6	10.9	10.5	23.0
HSA : Pt^{4+} = 1 : 8	54.9	11.5	10.0	23.6
HSA : Pt^{4+} = 1 : 10	52.6	13.0	9.1	25.3

spectra and contour ones are shown in Fig. 7. Four peaks can be seen in Fig. 7. The peak where $\lambda_{ex} = \lambda_{em}$ is the first-ordered Rayleigh scattering (RLS) peak. Peak a (λ_{ex} = 280 nm, λ_{em} = 334 nm) relates to the fluorescence behavior of Trp and Tyr residues; peak b (λ_{ex} = 230 nm, λ_{em} = 335 nm) mainly reveals the fluorescence spectral behavior of the polypeptide backbone structure, and its fluorescence intensity is correlated with the secondary structure of protein.[26,27] The production of RLS is correlated with the formation of certain aggregates and primarily the particle dimension of the formed aggregate in solution dominates the RLS intensity. Bearing these points in mind, it is inferred from the results that the size of the HSA–Pt^{4+} compound complexes may be not changed obviously comparing that of HSA, for the peak intensity are all around 2000. Analyzing from the intensity changes of peak a and peak b, they decreased obviously in the presence of the Pt^{4+} compound, the fluorescence intensity ratios of peak a and peak b are 1.70 : 1 and 1.27 : 1, respectively.

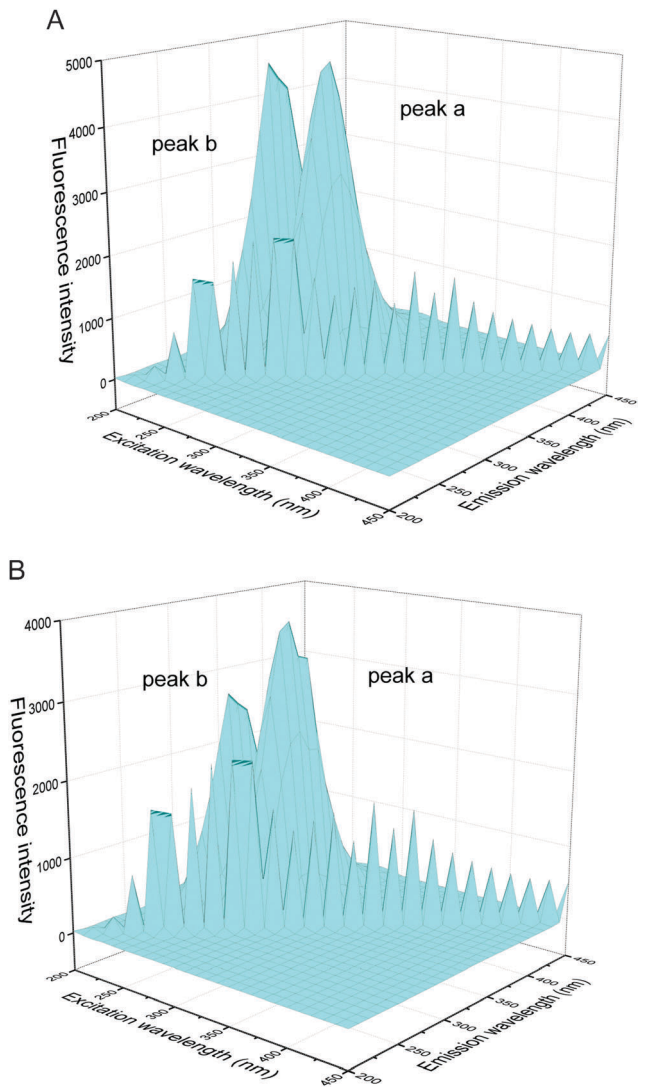

Fig. 7 The three-dimensional fluorescence spectra of the HSA–Pt^{4+} compound system. Conditions: T = 300 K, pH 7.4, salt concentration 0.9%.; c(HSA) = 1.0 × 10^{-6} M; c(Pt(VI)): 0 (A) and 14.0 (B) ×10^{-6} M.

The above phenomena and analysis of the fluorescence characteristic of the peaks revealed that the binding site is near Trp and Tyr residues and induced the fluorescence quenching of intrinsic fluorescence of HSA.[29,30] The binding of the Pt^{4+} compound induced slight unfolding of the polypeptides of protein.

3.5. The Pt^{4+} compound was located at site I of HSA

To study the distinct binding site of the Pt^{4+} compound on HSA, site-specific ligands were used: warfarin and furosemide for site I and ibuprofen for site II.[28] Fig. 8A shows that the fluorescence intensity significantly decreased after the addition of warfarin and furosemide but not after adding ibuprofen, suggesting that the Pt^{4+} compound binds to site I of HSA. It could be presumed that the Pt^{4+} compound is situated in the binding cavity of the

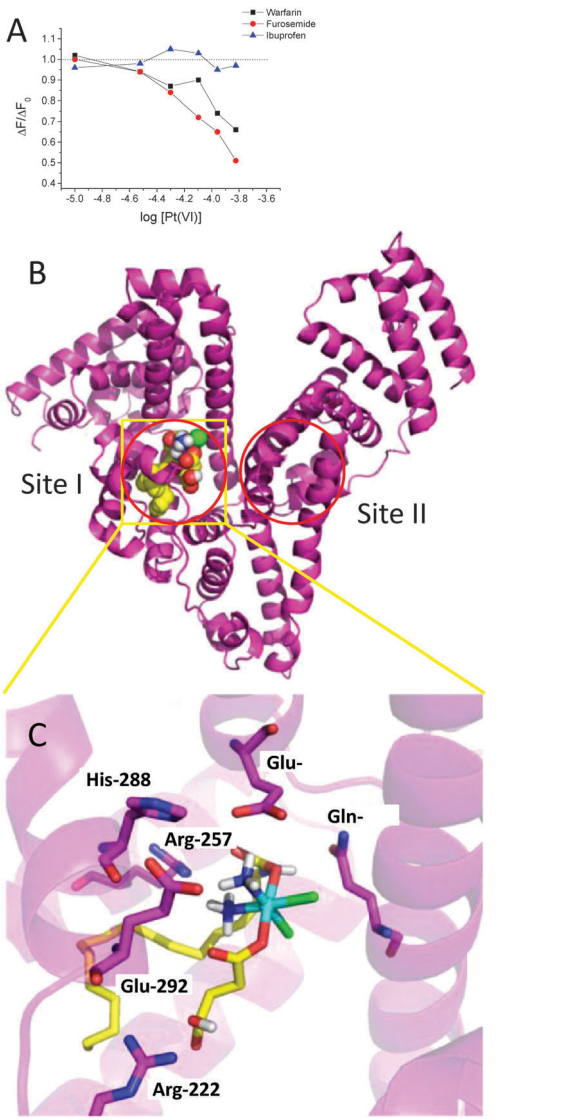

Fig. 8 (A) Molecular probing experiment showing site I is the major binding site. Concentration of the probe molecules is fixed at 1.0 × 10^{-6} M, pH = 7.4, salt concentration 0.9%. Molecular docking results of the HSA–Pt^{4+} compound interacting: (B) location of the compound in HSA showing that the main binding site is site I; (C) amino acid residues around 4 Å of the Pt^{4+} compound molecule.

site I and negative carbonyl groups may slightly interact with positively charged residues such as Lys-195, Lys-199, Arg-218, Arg-222, His-242, and Arg-257 which are located at the entrance of the site I cavity.

The molecular docking has been employed to further understand precisely the binding site of the Pt^{4+} compound and HSA. HSA comprises of three homologous domains (I–III): I (residues 1–195), II (196–383), III (384–585), each domain comprises of subdomains that posses common structural motifs. The principal regions of ligand binding to HSA are located in hydrophobic cavities of subdomains IIA and IIIA, which are consistent with Sudlow sites I and II, respectively. In the present study, Autodock program is applied to calculate the possible conformation of the Pt^{4+} compound that binds to the protein. Fig. 8C shows that the Pt^{4+} compound more favorably fits in the cavity of subdomains IIA, which corresponds to site I. His-288, Glu-153, Arg-257, Gln-196, Glu-292 and Arg-222 of site I were around the 4 Å of the compound, of which Arg-257, Arg-222 and His-288 may be involved in the electrostatic interaction.

4. Conclusions

In this paper, a potential anti-hepatoma drug *cis*,*cis*,*trans*-$[Pt(NH_3)_2Cl_2(O_2CCH_2CH_2COOH)$-$(OCONHC_{16}H_{33})]$ was synthesized and it showed excellent anti-liver cancer activity. The interaction of human serum albumin and the compound was investigated employing different spectroscopic and molecular docking techniques. The results revealed that the secondary structure of protein was affected upon interaction with the compound. Fluorescence results indicated the presence of the static quenching mechanism in the binding of the Pt^{4+} compound to the protein. Based on spectral data we have concluded that the Pt^{4+} compound bound to site I of protein, which is located in the hydrophobic pocket of subdomain IIA.

Acknowledgements

This work was supported by grants from Medical and Technologic Development Project of Shandong province (2011QZ028). The authors thank Dr Yamin Chang for his technical support in Pt^{4+} compound synthesis and Dr James. H. Haywood of Michigan State University for editing the manuscript.

References

1 B. A. Costello, M. J. Borad, Y. Qi, G. P. Kim, D. W. Northfelt, C. Erlichman and S. R. Alberts, *Invest. New Drugs*, 2014, **32**, 710–716.
2 J. Balmana, N. M. Tung, S. J. Isakoff, B. Grana, P. D. Ryan, C. Saura, E. S. Lowe, P. Frewer, E. Winer, J. Baselga and J. E. Garber, *Ann. Oncol.*, 2014, **25**, 1656–1663.
3 G. Freyer, N. Isambert, B. You, S. Zanetta, C. Falandry, L. Favier, V. Trillet-Lenoir, S. Assadourian, K. Soussan-Lazard, S. Ziti-Ljajic and P. Fumoleau, *Br. J. Cancer*, 2012, **107**, 598–603.
4 S. Huo, J. Dong, S. Shen, Y. Ren, C. Song, J. Xu and T. Shi, *Dalton Trans.*, 2014, **43**, 15328–15336.
5 V. Novohradsky, L. Zerzankova, J. Stepankova, O. Vrana, R. Raveendran, D. Gibson, J. Kasparkova and V. Brabec, *J. Inorg. Biochem.*, 2014, **140**, 72–79.
6 T. Fojo, N. Farrell, W. Ortuzar, H. Tanimura, J. Weinstein and T. G. Myers, *Crit. Rev. Oncol. Hematol.*, 2005, **53**, 25–34.
7 N. Graf, D. R. Bielenberg, N. Kolishetti, C. Muus, J. Banyard, O. C. Farokhzad and S. J. Lippard, *ACS Nano*, 2012, **6**, 4530–4539.
8 A. V. Klein and T. W. Hambley, *Chem. Rev.*, 2009, **109**, 4911–4920.
9 Z. Cheng, Y. Dai, X. Kang, C. Li, S. Huang, H. Lian, Z. Hou, P. Ma and J. Lin, *Biomaterials*, 2014, **35**, 6359–6368.
10 P. J. Bednarski, K. Korpis, A. F. Westendorf, S. Perfahl and R. Gruenert, *Philos. Trans. R. Soc., A*, 2013, **371**, 20120118.
11 X. C. Zhao and R. T. Liu, *Environ. Int.*, 2012, **40**, 244–255.
12 M. Marszalek, A. Konarska, E. Szajdzinska-Pietek and M. Wolszczak, *J. Phys. Chem. B*, 2013, **117**, 15987–15993.
13 R. Kato, Y. Kobayashi, M. Akiyama and T. Komatsu, *Dalton Trans.*, 2013, **42**, 15889–15892.
14 S. Dhar, W. L. Daniel, D. A. Giljohann, C. A. Mirkin and S. J. Lippard, *J. Am. Chem. Soc.*, 2009, **131**, 14652–14653.
15 D. P. Yeggoni and R. Subramanyam, *Mol. BioSyst.*, 2014, **10**, 3101–3110.
16 M. S. S. Dorraji, V. P. Azar and M. H. Rasoulifard, *Eur. J. Pharm. Sci.*, 2014, **64**, 9–17.
17 N. V. Rakotoarivelo, P. Perio, E. Najahi and F. Nepveu, *J. Phys. Chem. B*, 2014, **118**, 13477–13485.
18 Y. Zhu, R. Zhang, Y. Wang, J. Ma, K. Li and Z. Li, *J. Photochem. Photobiol., B*, 2014, **140**, 381–389.
19 C. Hebia, L. Bekale, P. Chanphai, J. Agbebavi and H. A. Tajmir-Riahi, *J. Photochem. Photobiol., B*, 2014, **130**, 254–259.
20 S. Dubeau, P. Bourassa, T. J. Thomas and H. A. Tajmir-Riahi, *Biomacromolecules*, 2010, **11**, 1507–1515.
21 Y. J. Hu, Y. Liu and X. H. Xiao, *Biomacromolecules*, 2009, **10**, 517–521.
22 X. Zhao, F. Sheng, J. Zheng and R. Liu, *J. Agric. Food Chem.*, 2011, **59**, 7902–7909.
23 R. Sindhu, A. K. Tiwari, L. C. Mishra and M. M. Husain, *Cancer Biother. Radiopharm.*, 2012, **27**, 452–456.
24 S. Tabassum, W. M. Al-Asbahy, M. Afzal and F. Arjmand, *J. Photochem. Photobiol., B*, 2012, **114**, 132–139.
25 X. Zhao, D. Lu, F. Hao and R. Liu, *J. Hazard. Mater.*, 2015, **292**, 98–107.
26 M. Maciazek-Jurczyk, *Pharmacol. Rep.*, 2014, **66**, 727–731.
27 S. Jana, S. Dalapati, S. Ghosh and N. Guchhait, *Biopolymers*, 2012, **97**, 766–777.
28 J. N. Tian, J. Q. Liu, W. Y. He, Z. D. Hu, X. J. Yao and X. G. Chen, *Biomacromolecules*, 2004, **5**, 1956–1961.
29 A. Varlan, S. Ionescu and M. Hillebrand, *Luminescence*, 2011, **26**, 710–715.
30 X. Zhao, R. Liu, Y. Teng and X. Liu, *Sci. Total Environ.*, 2011, **409**, 892–897.

